Journal of Applied Fluid Mechanics, Vol. 15, No. 4, pp. 1207-1220, 2022.
Available online at www.jafmonline.net, ISSN 1735-3572, EISSN 1735-3645.
https://doi.org/10.47176/jafm.15.04.1063

Mixed Convection Magnetic Nanofluid Flow past a Rotating Vertical Porous Cone

N. S. Wahid[1†], N. Md Arifin[1,2], N. S. Khashi'ie[3], I. Pop[4], N. Bachok[1,2], M. E. Hafidz Hafidzuddin[5]

[1]*Department of Mathematics and Statistics, Faculty of Science Universiti Putra Malaysia, 43400 UPM Serdang, Selangor, Malaysia*
[2]*Institute for Mathematical Research, Universiti Putra Malaysia, 43400 UPM Serdang, Selangor, Malaysia*
[3]*Fakulti Teknologi Kejuruteraan Mekanikal dan Pembuatan, Universiti Teknikal Malaysia Melaka, Hang Tuah Jaya, 76100 Durian Tunggal, Melaka, Malaysia*
[4]*Department of Mathematics, Babeş-Bolyai University, R-400084 Cluj-Napoca, Romania*
[5]*Centre of Foundation Studies for Agricultural Science, Universiti Putra Malaysia,43400 UPM Serdang, Selangor, Malaysia*

†*Corresponding Author Email: gs58394@student.upm.edu.my*

(Received December 27, 2021; accepted April 16, 2022)

ABSTRACT

Magnetic nanofluids (MNFs) have been the focus of extensive research nowadays owing to their potential usefulness as a transfer medium. This study is concerned with the boundary layer flow and heat transfer of MNF past a rotating vertical cone with the embedment of the porosity regime and mixed convection. The buoyancy opposing flow on the combined free and forced convection is being emphasized in this study to evaluate the behavior of the fluid within this region and predict the point of the boundary layer transition. The initial formulation of the model is simplified appropriately by employing the suitable similarity transformation. The package of bvp4c MATLAB is employed to execute the numerical solutions. Analysis of stability is also reported. Due to the mixed convection parameter, the opposing flow contributes towards two different alternative solutions, but the second solution is not stable. A higher local Nusselt number are achieved by increasing the concentration of magnetic nanofluid up to 2% and enlarging the mixed convection parameter under the influence of the porosity regime in the vertical rotating cone. It has been established in this study that the addition of cobalt ferrite as the magnetic nanoparticles (MNPs) is proven to have the ability in enhancing the thermal performance of the fluid.

Keywords: Mixed convection; Nanofluid; Porous medium; Cone; Stability analysis.

NOMENCLATURE

C_{fx}, C_{fy}	skin friction in x, y -directions	ε	porosity parameter
Da^{-1}	inverse Darcy number	β_f	thermal expansion of base fluid
f_c	friction factor	β_{nf}	thermal expansion of nanofluid
Gr_L	Grashof number	β_s	thermal expansion of nanoparticle
K	permeability parameter	γ	eigenvalue parameter
k_f	thermal conductivity of base fluid	λ	mixed convection parameter
k_{nf}	thermal conductivity of nanofluid	μ_f	dynamic viscosity of base fluid
k_s	thermal conductivity of nanoparticle	μ_{nf}	dynamic viscosity of nanofluid
L	characteristic length of cone	ρ_f	density of base fluid
Nu_x	local Nusselt number	ρ_{nf}	density of nanofluid
Pr	Prandtl number	ρ_s	density of nanoparticle
r	cone radius	$(\rho C_p)_f$	heat capacity of base fluid
Re_L	Reynolds number		

T_w	cone surface temperature
T_∞	free stream temperature
T_0	characteristic temperature
t	time
u, v, w	velocity in x, y, z -directions
$(\rho C_p)_{nf}$	heat capacity of nanofluid
$(\rho C_p)_s$	heat capacity of nanoparticle
τ	dimensionless time variable
ϕ	nanoparticle volume fraction
Ω	angular velocity

1. INTRODUCTION

The urgent demand for heat exchangers and coolants with enhanced performance has led to the innovation of nanofluid. This fluid consists of the colloidal diffusion of solid particles of nano-sized that are suspended in a carrier fluid. The original idea of solid particle dispersion was first developed by Maxwell (1873) to augment the thermal properties. However, because of the size of the solid particles, mostly in micro-sized; clogging and sedimentation in the flow passage have become a challenge due to the agglomeration among the solid particles (Ali *et al*., 2018). For that reason, Choi and Eastman (1995) came up with the idea of utilizing smaller size solid particles, which are nanoparticles, to overcome this issue. Several reviews in myriad aspects of nanofluid are available in this literature for further reading: (see Saidur *et al*., 2011; Yu and Xie, 2012; Akilu *et al*., 2016; Devendiran and Amirtham, 2016; Prasad *et al*., 2017; Ahmadi *et al*., 2018).

Magnetic nanofluid (MNF), also known as a ferrofluid, is one of the reliable emerging types of nanofluid that receive great interest among researchers due to its special magnetic features. MNF is made up of the stable colloidal mixtures of superparamagnetic nanoparticles such as iron and cobalt (ferromagnetic material), as well as magnetite (ferromagnetic material) that is dispersed in a non-magnetic carrier fluid viz. oil, water, or ethylene glycol (Genc & Derin, 2014; Nkurikiyimfura *et al*., 2013). Historically, this fluid was initially suggested by Steve Papell (at NASA) to make a suitable liquid rocket fuel suspended with finely-ground iron oxide (Stephen, 1965). Since then, this fluid has been used to solve many complex activities, including in biomedical (e.g., drug delivery, contrast agent/tracer, magnetic resonance image technology (MRI)), thermal engineering (e.g., thermal conductivity, heat transfer enhancement), and machine/device design (e.g., inertia damper, magnetic sealing, lubrication, film bearing, loudspeaker) applications (Marszałł, 2011; Khairul *et al*., 2017; Kumar & Subudhi, 2018; Kole & Khandekar, 2021).

Multidisciplinary strategies are required to understand the properties of MNF. One of them is by studying its flow dynamic and heat transfer properties at the boundary layer so that the flow can be modelled and controlled accordingly when applied to a specific application. Qasim *et al*. (2014) examined the heat transmission performance at the boundary layer of magnetite-water MNF along an expanding cylinder. The local Nusselt number for this fluid increases and aligns with the non-magnetic (alumina-water) nanofluid only if the extra magnetic field is applied. Though the non-magnetic nanoparticle has a higher thermal conductivity than the magnetic nanoparticle, the performance of MNF can be manipulated with the external magnetic field. Another comparison study between MNF dan non-MNF was also conducted by Gul *et al*. (2015) with the inclusion of an external magnetic field and mixed convection along a vertical channel. The temperature distribution of MNF is observed to be lower than non-MNF, but the temperature distribution can be improved by magnifying the magnetic nanoparticles concentration. Their findings align with the prior experimental studies examined by Colla *et al*. (2012). Later, Raju and Sandeep (2017) evaluate the unsteady MNF with water-based cobalt ferrite nanoparticles by using Casson model. They concluded that the spike in the concentration of the nanoparticles and buoyancy had initiated the skin friction to get larger.

Jusoh *et al*. (2018) employed three different base liquids towards the magnetite MNF in their study on the rotating flow past the exponentially expanding/contracting sheet. The MNF with kerosene as the base liquid is calculated to have the highest heat transfer efficiency compared to water and methanol. Besides, Sulochana *et al*. (2018) also considered magnetite-water and magnetite-methanol as the MNF to be investigated in the moving horizontal needle. Ahmed *et al*. (2019) researched the radiative MNF flow over a wedge for several base liquids and nanoparticles. The stagnation point flow with Newtonian heating of magnetite nanofluid was disclosed by Mohamed *et al*. (2019). Magnetite, cobalt ferrite, and manganese-zinc ferrite nanoparticles are adopted by Bognár and Hriczó (2020) to explore the boundary layer flow of MNF past an expanding flat sheet. Khan *et al*. (2020) revealed the characteristic of micropolar MNF of second-order velocity slip flow through a two-phase model due to a stretchable surface. Rasli and Ramli (2021) addressed the study on MNF with three different magnetic nanoparticles over the exponentially stretchable/shrinkable sheet with magnetohydrodynamic. Recently, Anuar *et al*. (2021) contemplated the flow of hybrid MNF with heat source/sink due to the stagnation point on a stretchable and shrinkable sheet. The viscous dissipation effect has been used by Hamid *et al*. (2022) to explore the flow phenomena of dusty MNF on the non-isothermal movable surface. Several other latest pertinent studies on MNF are extractable through this list: (Bhandari, 2021; Jalili *et al*., 2021; Mohamed *et al*., 2021; Nayak *et al*., 2021; Saranya *et al*., 2021; Uddin *et al*., 2021).

Furthermore, instead of suspending stronger thermal conductivity nanoparticles towards the base fluid, changing the flow geometry is also one of the

techniques that could be utilized to improve the heat transfer performance. Karuppasamy *et al.* (2020) concluded that the cone shape inserts in the heat exchanger tube significantly improve the heat transfer process. Historically, the work on vertical cone was pioneered by Kumari *et al.* (1989) to elucidate the flow and heat transfer for mixed convection. Since then, the utilization of cone geometry has been considered by many researchers to investigate its effectiveness either by using the numerical or experimental approach. The modified rotating reactor with a cone shape has been developed by Guoxin *et al.* (2008) for the thermochemical treatment of coal with a solid heat carrier. The conical shape coil with different cone angles was also used by Purandare *et al.* (2015) to analyze the thermal capability of the heat exchanger. Palanisamy & Mukesh Kumar (2019) experimented the heat transfer in the heat exchanger that made up of cone helically coiled tube with the inclusion of nanofluid. The exploration on nanofluid flooding effect for the recovery oil process enhancement by using the incomplete porous cone was experimented by Hemmat Esfe *et al.* (2020). This kind of geometry has captivated the interest of many researchers since it is practically important in real applications. To name a few, it is utilized in space technology, automotive, nuclear safety management, biomedical, aerospace, heat exchanger, oil recovery, and radiology (Raju *et al.*, 2017).

The investigations as mentioned previously are diversified accordingly with different kind of effects and geometries to simulate the behavior of MNF in actual boundary layer phenomena. Furthermore, so far, we have witnessed that the numerical investigation on mixed convection magnetic nanofluid (MNF) flow past a rotating vertical porous cone has not yet been addressed. Hence, we believed that this study could fill the research gap significantly with its originality for future insight. The highlights of the addressed study are listed as follows:

- We consider the inclusion of cobalt ferrite-water ($CoFe2O_4$-H_2O) MNF to extend the previous study by Mallikarjuna *et al.* (2016) as their study is only limited to a regular viscous fluid.
- The Tiwari and Das model for nanofluid is considered in this study instead of Buongiorno model.
- The mixed convection with opposing flow is considered, while the study by Mallikarjuna *et al.* (2016) only emphasized the assisting flow.
- The trusted solver (bvp4c MATLAB) is implemented to solve the flow problem, and the results are validated with several existing studies.
- Dual solutions are presented together with the critical point of the boundary layer separation.
- The study is completed with stability analysis in providing the conclusion about the stability feature of the generated dual solutions.
- The increment of $CoFe2O_4$ volume fraction up to 2% is numerically verified to enhance the local Nusselt number.

2. MATHEMATICAL MODEL

As visualized in Fig. 1, the mixed convection MNF flow past a vertical rotating cone in a porous medium with an angular velocity Ω is considered, where x-axis is along a meridional section, y-axis is along a circular section, and the z-axis is normal to the cone surface. Other assumptions that we intend to make are:

- The flow is steady and laminar being at $z \geq 0$.
- Cobalt ferrite and water are chosen as the magnetic nanoparticles (MNPs) and the base liquid, respectively, to form MNF.
- The cone surface is preserved at a temperature $T_w(x) = T_\infty + T_0(x/L)$, where T_0 is a characteristic temperature of the fluid, with $T_0 > 0$ for the assisting flow, $T_0 < 0$ for the opposing flow and $T_0 = 0$ for the forced convection flow, and T_∞ is the free-stream temperature, while L is the characteristic length of the cone.
- The porous medium is in the local thermal equilibrium.

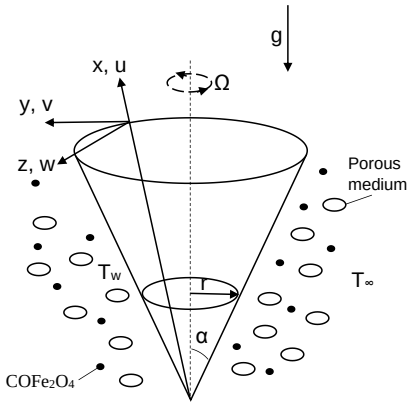

Fig. 1. Model illustration with coordinate system.

Keeping these assumptions in mind, and with the reference from Mallikarjuna *et al.* (2016) and Ahmed *et al.* (2019), the mathematical model are formulated as

$$\frac{\partial u}{\partial x} + \frac{\partial w}{\partial z} + \frac{u}{x} = 0 \tag{1}$$

$$\varepsilon^{-2}\left(u\frac{\partial u}{\partial x} + w\frac{\partial u}{\partial z} - \frac{v^2}{x}\right) = \varepsilon^{-1}\frac{\mu_{nf}}{\rho_{nf}}\frac{\partial^2 u}{\partial z^2} - \frac{\mu_{nf}}{\rho_{nf}}\frac{u}{K} + \frac{(\rho\beta)_{nf}}{\rho_{nf}}(T - T_\infty)g\cos\alpha \tag{2}$$

$$\varepsilon^{-2}\left(u\frac{\partial v}{\partial x} + w\frac{\partial v}{\partial z} + \frac{uv}{x}\right) = \varepsilon^{-1}\frac{\mu_{nf}}{\rho_{nf}}\frac{\partial^2 v}{\partial z^2} - \frac{\mu_{nf}}{\rho_{nf}}\frac{v}{K} \tag{3}$$

$$u\frac{\partial T}{\partial x}+w\frac{\partial T}{\partial z}=\frac{k_{nf}}{\left(\rho C_p\right)_{nf}}\frac{\partial^2 T}{\partial z^2} \tag{4}$$

subject to

$$\left.\begin{aligned} &v=\Omega r,\ u=0,\ w=0,\\ &T=T_w(x)=T_\infty+T_0\left(\frac{x}{L}\right)\end{aligned}\right\}\ \text{at}\ z=0$$
$$u\to 0,\ v\to 0,\ T\to T_\infty\ \text{as}\ z\to\infty \tag{5}$$

where u, v and w are the velocity components along x, y, z directions, $r=x\sin\alpha$ is the radius of the cone at the base $(x=L)$, ε is the porosity parameter and K is the porous medium permeability.

It should be noted that the MNF in this study considers the thermophysical properties such as, density ρ_{nf}, heat capacity $\left(\rho C_p\right)_{nf}$, dynamic viscosity μ_{nf}, thermal conductivity k_{nf}, and thermal expansion β_{nf} which the correlations are given in Table 1 (Takabi & Salehi, 2015). The subscript of f and s refer to the base liquid and MNP, separately. The thermal and physical characteristics for base liquid and MNP are given in Table 2 (Ahmed *et al*., 2019; Raju & Sandeep, 2017; Gul *et al*., 2015), where ϕ is the MNP volume fraction and $\mathrm{Pr}=\nu_f\left(\rho C_p\right)_f/k_f$ is Prandtl number.

Table 1 Correlation of thermophysical properties of MNF

Properties	Correlations
Density	$\rho_{nf}=(1-\phi)\rho_f+\phi\rho_s$
capacity Heat	$\left(\rho C_p\right)_{nf}=(1-\phi)\left(\rho C_p\right)_f+\phi\left(\rho C_p\right)_s$
Dynamic viscosity	$\frac{\mu_{nf}}{\mu_f}=\frac{1}{(1-\phi)^{2.5}}$
Thermal conductivity	$\frac{k_{nf}}{k_f}=\frac{k_s+2k_f-2\phi\left(k_f-k_s\right)}{k_s+2k_f+\phi\left(k_f-k_s\right)}$
Thermal expansion	$\beta_{nf}=\frac{1}{\rho_{nf}}\left(\phi\rho_s\beta_s+(1-\phi)\rho_f\beta_f\right)$

Table 2 Thermal and physical characteristics for MNF compositions

Properties	Water (H_2O)	Cobalt ferrite ($CoFe_2O_4$)
$\rho\left(\mathrm{kg/m^3}\right)$	997.1	4907
$C_p\left(\mathrm{J/kgK}\right)$	4179	700
$k\left(\mathrm{W/mk}\right)$	0.613	3.7
$\beta(1/K)$	21×10^{-5}	2.1×10^{-5}
Pr	6.96	-
ϕ	-	1%-2%

The boundary conditions Eq. (5) suggest the following similarity variables (Mallikarjuna *et al*., 2016)

$$\begin{aligned} &u=x\Omega\sin\alpha\, f(\eta),\ v=x\Omega\sin\alpha\, g(\eta),\\ &w=\sqrt{\nu_f\Omega\sin\alpha}\,h(\eta),\\ &\theta(\eta)=\frac{T-T_\infty}{T_w-T_\infty},\ \eta=z\sqrt{\Omega\sin\alpha/\nu_f}\end{aligned} \tag{6}$$

where prime denotes the differentiation of the function concerning η.

Applying the transformation into Eqs. (1) to (5), we get the new transformed equations

$$f=-\frac{1}{2}h' \tag{7}$$

$$\begin{aligned} &\varepsilon^{-1}\left(\frac{\mu_{nf}/\mu_f}{\rho_{nf}/\rho_f}\right)h'''-\varepsilon^{-2}hh''\\ &-\left(\frac{\mu_{nf}/\mu_f}{\rho_{nf}/\rho_f}\right)Da^{-1}h'+\varepsilon^{-2}\left(\frac{1}{2}h'^2-2g^2\right)\\ &-2\frac{\beta_{nf}}{\beta_f}\lambda\theta=0\end{aligned} \tag{8}$$

$$\begin{aligned} &\varepsilon^{-1}\left(\frac{\mu_{nf}/\mu_f}{\rho_{nf}/\rho_f}\right)g''-\varepsilon^{-2}\left(hg'-h'g\right)\\ &-\left(\frac{\mu_{nf}/\mu_f}{\rho_{nf}/\rho_f}\right)Da^{-1}g=0\end{aligned} \tag{9}$$

$$\begin{aligned} &\frac{1}{\mathrm{Pr}}\frac{k_{nf}/k_f}{\left(\rho C_p\right)_{nf}/\left(\rho C_p\right)_f}\theta''-h\theta'\\ &+\frac{1}{2}h'\theta=0\end{aligned} \tag{10}$$

subject to the boundary conditions

$$\left.\begin{aligned} &h(0)=0,\ h'(0)=0,\ g(0)=1,\ \theta(0)=1\\ &h'(\eta)\to 0,\ g(\eta)\to 0,\\ &\theta(\eta)\to 0\end{aligned}\right\}\ \text{as}\ \eta\to\infty, \tag{11}$$

where, Da^{-1} is the inverse Darcy number and λ is the mixed convection parameter, which mathematically expressed as

$$Da^{-1}=\frac{\nu_f}{K\Omega\sin\alpha},\ \lambda=\frac{Gr_L}{\mathrm{Re}_L^2} \tag{12}$$

with $Gr_L=g\beta_f\left(T_w-T_\infty\right)\cos\alpha\, L^3/\nu_f^2$ as the Grashof number and $\mathrm{Re}_L=\Omega L^2\sin\alpha/\nu_f$ as the Reynolds number. The constant mixed convection parameter is denoted by λ with $\lambda>0$ for assisting flow, $\lambda<0$ for opposing flow and $\lambda=0$ for forced convection flow. The opposing flow will be the main focus.

The skin friction coefficients C_{fx}, C_{fy}, and the local Nusselt number Nu_x, are equated as (Hering & Grosh, 1963):

$$C_{fx}=\frac{2\mu_{nf}}{\rho_f u_w^2(x)}\left(\frac{\partial u}{\partial z}\right)_{z=0},$$
$$C_{fy}=\frac{2\mu_{nf}}{\rho_f v_w^2(x)}\left(\frac{\partial v}{\partial z}\right)_{z=0},$$
$$Nu_x=-\frac{xk_{nf}}{k_f(T_w-T_\infty)}\left(\frac{\partial T}{\partial z}\right)_{z=0}. \tag{13}$$

Using Eq. (6) and Eq. (13) we get

$$\mathrm{Re}_L^{1/2}C_{fx}=-\frac{\mu_{nf}}{\mu_f}h''(0),$$
$$2^{-1}\mathrm{Re}_L^{1/2}C_{fy}=\frac{\mu_{nf}}{\mu_f}g'(0), \tag{14}$$
$$\mathrm{Re}_L^{-1/2}Nu_x=-\frac{k_{nf}}{k_f}\theta'(0).$$

3. STABILITY ANALYSIS

As two non-identical solutions are perceived to be executed in this study, here, we include the stability analysis to evaluate and validate the feature of the solutions. This analysis has been initiated by Merkin (1986) and extensively followed by other researchers (Khashi'ie *et al*., 2021; Mabood & Akinshilo, 2021; Tshivhi & Makinde, 2021; Wahid *et al*., 2021; Yahaya *et al*., 2021; Kolsi *et al*., 2021; Aladdin & Bachok, 2021). To analyze the stability, we first need to set Eqs. (2)-(4) to be unsteady and introducing the following newly similarity transformation,

$$\begin{aligned}&u=x\Omega\sin\alpha\, f(\eta,\tau),\\&v=x\Omega\sin\alpha\, g(\eta,\tau),\\&w=\sqrt{\nu_f\Omega\sin\alpha}\,h(\eta,\tau),\\&\theta(\eta,\tau)=\frac{T-T_\infty}{T_w-T_\infty},\\&\eta=z\sqrt{\Omega\sin\alpha/\nu_f},\ \tau=t\Omega\sin\alpha\end{aligned} \tag{15}$$

where τ is the non-dimensional time variable with time t. Hence, applying this transformation towards the unsteady equations, we then obtain the subsequent form of equations

$$\begin{aligned}&\varepsilon^{-1}\left(\frac{\mu_{nf}/\mu_f}{\rho_{nf}/\rho_f}\right)\frac{\partial^3 h}{\partial\eta^3}-\varepsilon^{-2}h\frac{\partial^2 h}{\partial\eta^2}\\&-2\frac{\beta_{nf}}{\beta_f}\lambda\theta-\frac{\mu_{nf}/\mu_f}{\rho_{nf}/\rho_f}Da^{-1}\frac{\partial h}{\partial\eta}\\&-\frac{1}{2}\left(\frac{\partial^2 h}{\partial\eta\partial\tau}\right)+\varepsilon^{-2}\left(\frac{1}{2}\left(\frac{\partial h}{\partial\eta}\right)^2-2g^2\right)=0\end{aligned} \tag{16}$$

$$\begin{aligned}&\varepsilon^{-1}\left(\frac{\mu_{nf}/\mu_f}{\rho_{nf}/\rho_f}\right)\frac{\partial^2 g}{\partial\eta^2}-\varepsilon^{-2}\left(h\frac{\partial g}{\partial\eta}-\frac{\partial h}{\partial\eta}g\right)\\&-\left(\frac{\mu_{nf}/\mu_f}{\rho_{nf}/\rho_f}\right)Da^{-1}g-\left(\frac{\partial g}{\partial\tau}\right)=0\end{aligned} \tag{17}$$

$$\begin{aligned}&\frac{1}{\mathrm{Pr}}\frac{k_{nf}/k_f}{(\rho C_p)_{nf}/(\rho C_p)_f}\frac{\partial^2\theta}{\partial\eta^2}-h\frac{\partial\theta}{\partial\eta}\\&+\frac{1}{2}\frac{\partial h}{\partial\eta}\theta-\left(\frac{\partial\theta}{\partial\tau}\right)=0\end{aligned} \tag{18}$$

subject to

$$\left.\begin{aligned}&h(\eta,\tau)=0,\ \frac{\partial h}{\partial\eta}(\eta,\tau)=0,\\&g(\eta,\tau)=1,\ \theta(\eta,\tau)=1,\end{aligned}\right\}\ \text{at}\ \eta=0$$
$$\left.\begin{aligned}&\frac{\partial h}{\partial\eta}(\eta,\tau)\to 0,\ g(\eta,\tau)\to 0,\\&\theta(\eta,\tau)\to 0\end{aligned}\right\}\ \text{as}\ \eta\to\infty \tag{19}$$

According to Weidman *et al*. (2006), the following eigenvalue equations that consist of eigenvalue parameter γ should be applied towards the previous transformed equations in evaluating the stability of the solution,

$$\begin{aligned}&h(\eta,\tau)=h_0(\eta)+e^{-\gamma\tau}H(\eta),\\&g(\eta,\tau)=g_0(\eta)+e^{-\gamma\tau}G(\eta),\\&\theta(\eta,\tau)=\theta_0(\eta)+e^{-\gamma\tau}Q(\eta),\end{aligned} \tag{20}$$

where $H(\eta),G(\eta),Q(\eta)$ are relatively small to $h(\eta)=h_0(\eta),\ g(\eta)=g_0(\eta),\ \theta(\eta)=\theta_0(\eta)$, separately. Upon simplification, we obtain the linearized eigenvalue system as follows

$$\begin{aligned}&\varepsilon^{-1}\left(\frac{\mu_{nf}/\mu_f}{\rho_{nf}/\rho_f}\right)H'''-\varepsilon^{-2}(h_0H''+Hh_0'')\\&-\left(\frac{\mu_{nf}/\mu_f}{\rho_{nf}/\rho_f}\right)Da^{-1}H'\\&+\varepsilon^{-2}(h_0'H'-4g_0G)-2\frac{\beta_{nf}}{\beta_f}\lambda Q+\frac{1}{2}\gamma H'=0\end{aligned} \tag{21}$$

$$\begin{aligned}&\varepsilon^{-1}\left(\frac{\mu_{nf}/\mu_f}{\rho_{nf}/\rho_f}\right)G''\\&-\varepsilon^{-2}\left((h_0G'+Hg_0')-(h_0'G+H'g_0)\right)\\&-\left(\frac{\mu_{nf}/\mu_f}{\rho_{nf}/\rho_f}\right)Da^{-1}G+\gamma G=0\end{aligned} \tag{22}$$

$$\begin{aligned}&\frac{1}{\mathrm{Pr}}\frac{k_{nf}/k_f}{(\rho C_p)_{nf}/(\rho C_p)_f}Q''-(h_0Q'+H\theta_0')\\&+\frac{1}{2}(h_0'Q+H'\theta_0)+\gamma Q=0\end{aligned} \tag{23}$$

subject to

$$\begin{aligned}&H(0)=0,\ H'(0)=0,\ G(0)=0,\ Q(0)=0,\\&H''(0)=1\ \text{(additional)}\end{aligned}$$
$$\left.\begin{aligned}&H'(\eta)\to 0\ \text{(rest)},\\&G(\eta)\to 0,\\&Q(\eta)\to 0\end{aligned}\right\}\ \text{as}\ \eta\to\infty. \tag{24}$$

The stability of the solution is analyzed via the generation of an infinite number of eigenvalues $\gamma_1 < \gamma_2 < \gamma_3 \ldots < \gamma_{n-1} < \gamma_n$ where if $\gamma_1 > 0$, we consider the solution as stable, and if $\gamma_1 < 0$, the solution is considered as non-stable because of the initial broadening of perturbations. Since all conditions are homogenous, we need to rest one condition and enforce a new additional condition as stated in Eq. (24) to ensure a possible set of eigenvalues can be generated (Harris *et al*., 2009).

4. NUMERICAL COMPUTATION

The flow problem is resolved using bvp4c solver MATLAB. This solver employs a finite difference approach that utilizes the three-stage Lobatto IIIa collocation formula, yielding a continuous solution with fourth-order precision (Kierzenka & Shampine, 2001; Shampine *et al*., 2003, 2004). The general syntax of the solver is *sol = bvp4c (@OdeBVP, @OdeBC, solinit, options).* This syntax contains several important functions that contain the main equations, boundary conditions, the initial mesh points and solution approximation, and the optional integration parameter, respectively. The mesh point is used in the collocation method to divide the integration interval into smaller parts. The algorithm for the solver begins with:

(i) Variable declaration

(ii) Initialization

(iii) Domain discretization

(iv) Call bvp4c

(v) Solution evaluation using Deval function

(vi) Numerical solutions computation

The residual of the continuous solution is employed to guide mesh selection and error control. If the solution unable to meet the tolerance limit, the solver will modify the mesh and the process will be repeated.

Before utilizing the solver, the resulting equations Eqs. (8)-(10) subject to Eq. (11) should be transformed into first-order differential equations, where we assume $h = y(1)$, $h' = y(2)$, $h'' = y(3)$ $g = y(4)$, $g' = y(5)$, $\theta = y(6)$ and $\theta' = y(7)$ so that the resulting equations are rewritten as the following,

$$h''' = \frac{\varepsilon\begin{pmatrix}\varepsilon^{-2}y(1)y(3)+\left(\frac{\mu_{nf}/\mu_f}{\rho_{nf}/\rho_f}\right)Da^{-1}y(2)\\ -\varepsilon^{-2}\left(\frac{1}{2}y(2)y(2)-2y(4)y(4)\right)\\ +2\frac{\beta_{nf}}{\beta_f}\lambda y(6)\end{pmatrix}}{\left(\frac{\mu_{nf}/\mu_f}{\rho_{nf}/\rho_f}\right)}$$

$$g'' = \frac{\varepsilon}{\left(\frac{\mu_{nf}/\mu_f}{\rho_{nf}/\rho_f}\right)}\begin{pmatrix}\varepsilon^{-2}\left(y(1)y(5)-y(2)y(4)\right)\\ +\left(\frac{\mu_{nf}/\mu_f}{\rho_{nf}/\rho_f}\right)Da^{-1}y(4)\end{pmatrix}$$

$$\theta'' = \frac{1}{\frac{1}{\Pr}\frac{k_{nf}/k_f}{\left(\rho C_p\right)_{nf}/\left(\rho C_p\right)_f}}\begin{pmatrix}y(1)y(7)\\ -\frac{1}{2}y(2)y(6)\end{pmatrix} \tag{25}$$

subject to

$$ya(1), ya(2), ya(4)-1, ya(6)-1,\\ yb(2), yb(4), yb(6) \tag{26}$$

where *ya* and *yb* refer to the boundary conditions when $\eta = 0$ and $\eta \to \infty$, respectively. The thickness of the boundary layer $(\eta_\infty = 15)$, the value of the parameters, and the initial guesses need to be set up accordingly in the coding program to execute the appropriate numerical solutions. The initial guesses are quite important in generating the best solutions because the efficacy of the solver ultimately depends on the appropriateness of the selected initial guesses since this solver is an iterative scheme. The numerical solution is acceptable when it is asymptotically converged towards the boundary conditions, and there is zero warning/error so that the numerical solution complies with the specified tolerance limit.

Table 3 Comparison values when Pr = 7, λ=Da^{-1}=0 in the absence of porosity and MNPs ϕ=0

	Present	(Rashad *et al*., 2016)	(Hering & Grosh, 1963)
$-h''(0)$	1.020464858	1.0203	1.0205
$-g'(0)$	0.615921901	0.61583	0.61592
$-\theta'(0)$	0.428545552	0.42842	0.42852

Table 4 Comparison values when Pr = 1,2, λ=0.1, Da^{-1}=0 in the absence of porosity and MNPs ϕ=0

	Pr = 1	Pr = 2
$-h''(0)$	1.128544651 (1.12824)	1.111471509 (1.11203)
$-g'(0)$	0.648233892 (0.64374)	0.627816846 (0.63347)
$-\theta'(0)$	0.546775247 (0.54573)	0.740985139 (0.74502)

( ) refers to the solution reported by (Rashad *et al*., 2016)

For validation purposes, the precision of the present method is validated by contrasting the executed numerical solutions with the previous studies for certain limiting cases as can be observed in Tables 3 and 4. The solutions are compared for the case

limited to the absence of porosity parameter and the exclusion of MNP (regular fluid). As tabulated in the tables, the numerical solutions are seen to be aligned with the prior studies although they implement a different kind of method in solving the problem. This comparison shows the trustworthiness and accuracy of the implemented numerical method.

For the computation on conducting the stability analysis, the same procedure is needed to reduce the system of equations where the assumptions and modification are made as follows:

$$
\begin{aligned}
&h_0 = s(1),\ h_0' = s(2),\ h_0'' = s(3),\\
&g_0 = s(4),\ g_0' = s(5),\ \theta_0 = s(6),\ \theta_0' = s(7),\\
&H = y(1),\ H' = y(2),\ H'' = y(3),\\
&G = y(4),\ G' = y(5),\ Q = y(6),\ Q' = y(7),
\end{aligned}
$$

$$
H''' = \frac{\varepsilon\begin{pmatrix}\varepsilon^{-2}\left(s(1)y(3)+y(1)s(3)\right)\\ +\left(\dfrac{\mu_{nf}/\mu_f}{\rho_{nf}/\rho_f}\right)Da^{-1}y(2)\\ -\varepsilon^{-2}\left(s(2)y(2)-4s(4)y(4)\right)\\ +2\dfrac{\beta_{nf}}{\beta_f}\lambda y(6)-\dfrac{1}{2}\gamma y(2)\end{pmatrix}}{\left(\dfrac{\mu_{nf}/\mu_f}{\rho_{nf}/\rho_f}\right)}
$$

$$
G'' = \frac{\varepsilon\begin{pmatrix}\varepsilon^{-2}\begin{pmatrix}\left(s(1)y(5)+y(1)s(5)\right)\\ -\left(s(2)y(4)+y(2)s(4)\right)\end{pmatrix}\\ +\left(\dfrac{\mu_{nf}/\mu_f}{\rho_{nf}/\rho_f}\right)Da^{-1}y(4)-\gamma y(4)\end{pmatrix}}{\left(\dfrac{\mu_{nf}/\mu_f}{\rho_{nf}/\rho_f}\right)}
$$

$$
Q'' = \frac{1}{\dfrac{1}{\Pr}\dfrac{k_{nf}/k_f}{\left(\rho C_p\right)_{nf}/\left(\rho C_p\right)_f}}\begin{pmatrix}\left(s(1)y(7)+y(1)s(7)\right)\\ -\dfrac{1}{2}s(2)y(6)\\ -\dfrac{1}{2}y(2)s(6)\\ -\gamma y(6)\end{pmatrix} \tag{27}
$$

subject to

$$
\begin{aligned}
&ya(1), ya(2), ya(4), ya(6), ya(3)-1,\\
&yb(4), yb(6)
\end{aligned} \tag{28}
$$

5. RESULTS AND DISCUSSION

As previously stated, the numerical solutions have been validated with the preceding studies for certain limiting cases, and therefore in this section, we are confident in executing the numerical solutions for the case of MNF with the inclusion of the porosity regime. The MNF contains cobalt ferrite ($CoFe_2O_4$) and is dispersed into the base liquid which is water. This MNF formation ($CoFe_2O_4$-H_2O) is analyzed in terms of their skin friction and heat transfer performance with several changing parameters. The thermophysical characteristic of the respective components in the MNF are set as tabulated in Table 2, where the volume fraction of $CoFe_2O_4$ is investigated at the amount of 1% to 2%.

Figures 2-4 display the distributions of tangential $\mathrm{Re}_L^{1/2}C_{fx}$ and azimuthal $2^{-1}\mathrm{Re}_L^{1/2}C_{fy}$ skin friction coefficients, and the local Nusselt number $\mathrm{Re}_L^{-1/2}Nu_x$ against the mixed convection $(\lambda<0)$ with a different volume fraction of $CoFe_2O_4$. These distributions are calculated with a fixed value of inverse Darcy number $Da^{-1}=0.01$ and porosity parameter $\varepsilon=1$ to evaluate the impacts of the volume fraction of $CoFe_2O_4$ towards the physical quantities stated. As shown in the figures (Figs. 2-4) by the first solution, this study confirms the ability of MNP (i.e., $CoFe_2O_4$) in improving $\mathrm{Re}_L^{1/2}C_{fx}$ and $\mathrm{Re}_L^{-1/2}Nu_x$ (heat transfer rate) when its dispersion is gradually added towards the base liquid, but not for $2^{-1}\mathrm{Re}_L^{1/2}C_{fy}$.

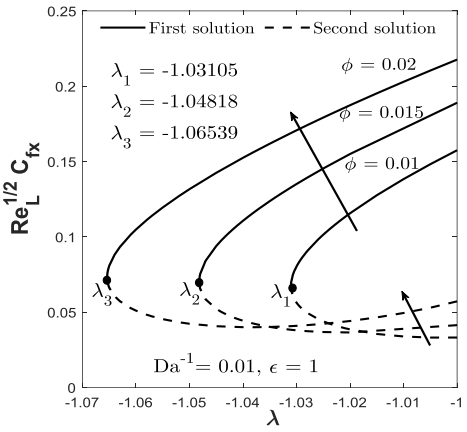

Fig. 2. Distribution of $\mathrm{Re}_L^{1/2}C_{fx}$ for different ϕ.

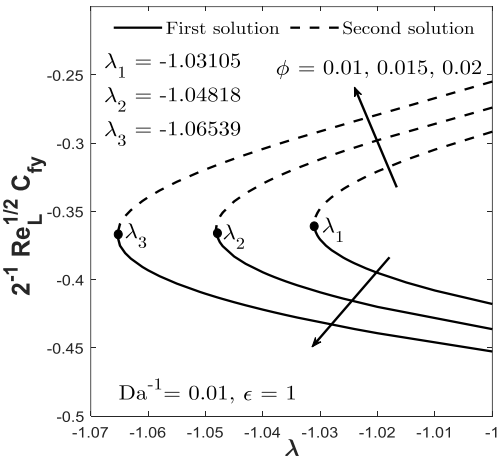

Fig. 3. Distribution of $2^{-1}\mathrm{Re}_L^{1/2}C_{fy}$ for different ϕ

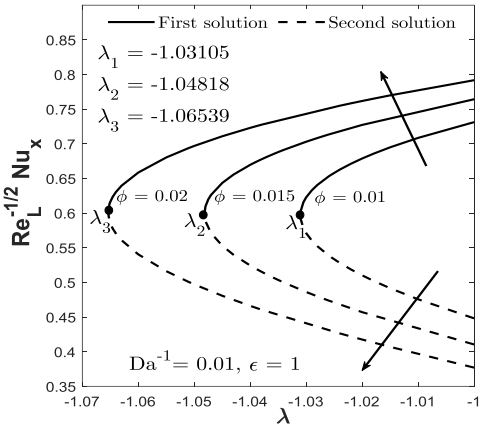

Fig. 4. Distribution of $\mathrm{Re}_L^{-1/2} Nu_x$ for different ϕ.

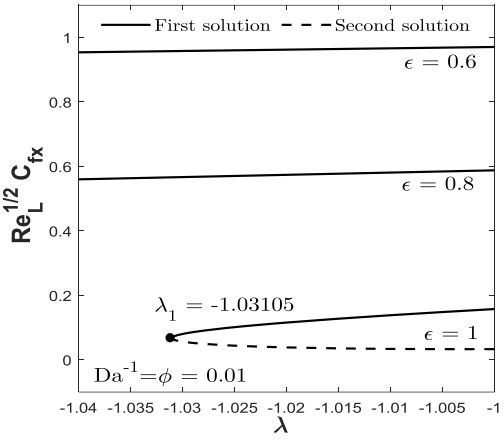

Fig. 5. Distribution of $\mathrm{Re}_L^{1/2} C_{fx}$ for different ε

Meanwhile, for the distributions of $2^{-1}\mathrm{Re}_L^{1/2} C_{fy}$ and $\mathrm{Re}_L^{-1/2} Nu_x$ in Figs. 3 and 4, the second solution shows the reflected pattern compared to its respective first solution as the volume fraction of $CoFe_2O_4$ increases. However, this second solution is validated to be non-stable when we evaluate its stability. The boundary layer separation for this case is seen to be located at the negative region of λ which is when the fluid experiencing the opposing flow due to the mixed convection. In particular, the critical point of the separation process takes place at $\lambda_{c1} = -1.03105$ $(\phi = 0.01)$ $\lambda_{c2} = -1.04818$ $(\phi = 0.015)$ and $\lambda_{c3} = -1.06539$ $(\phi = 0.02)$. Beyond this point, there is no feasible solution appeared. On a side note, this boundary layer separation from the state of laminar to turbulent would cause vibrations and obstruction in machinery and reduce the efficiency of the compressor if we consider it into practice (Gaviln, 2010). Therefore, to prevent such occurrence, this finding suggests increasing the volume fraction of $CoFe_2O_4$ or the mixed convection parameter accordingly. The flow is only favorable when $\lambda \geq \lambda_c$.

Figures 5-7 demonstrate the distributions of $\mathrm{Re}_L^{1/2} C_{fx}$, $2^{-1}\mathrm{Re}_L^{1/2} C_{fy}$ and $\mathrm{Re}_L^{-1/2} Nu_x$, separately, against $\lambda(<0)$ with a different value of ε when $\phi = Da^{-1} = 0.01$. In this case, the smaller value of ε is more dominant to improve $\mathrm{Re}_L^{1/2} C_{fx}$ and $\mathrm{Re}_L^{-1/2} Nu_x$ as can be contemplated from the first solution. Similar as Figures 2-4, the critical point for the separation process located at $\lambda_{c1} = -1.03105$ when $\varepsilon = 1$, while for the case when $\varepsilon = 0.6, 0.8$, the critical points should be further away $(\lambda_c < -1.03105)$. This also implies that the smaller porosity value would delay the separation process even better. The value of $\mathrm{Re}_L^{1/2} C_{fx}$, $2^{-1}\mathrm{Re}_L^{1/2} C_{fy}$ and $\mathrm{Re}_L^{-1/2} Nu_x$ can also be augmented by strengthening the mixed convection parameter for the first solution.

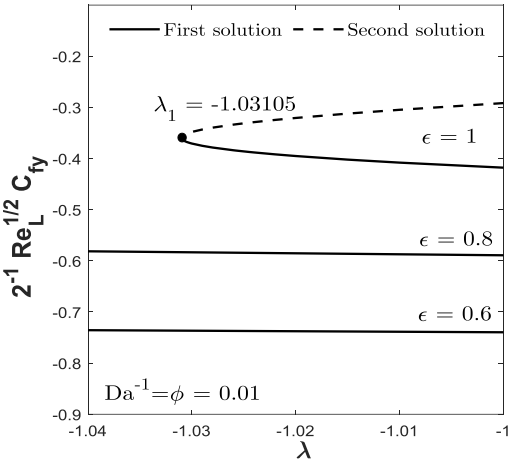

Fig. 6. Distribution of $2^{-1}\mathrm{Re}_L^{1/2} C_{fy}$ for different ε

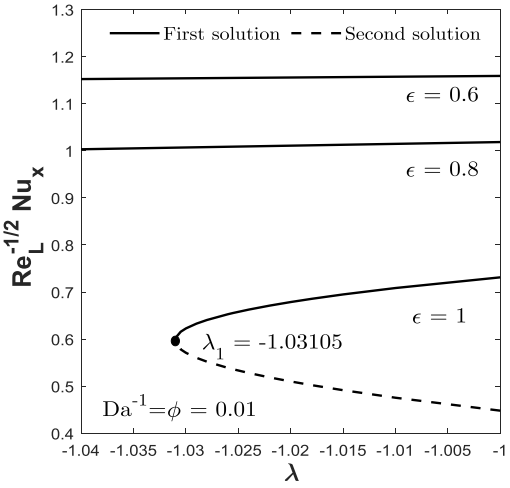

Fig. 7. Distribution of $\mathrm{Re}_L^{-1/2} Nu_x$ for different ε

Additionally, the distributions of $\mathrm{Re}_L^{1/2} C_{fx}$, $2^{-1}\mathrm{Re}_L^{1/2} C_{fy}$ and $\mathrm{Re}_L^{-1/2} Nu_x$ against $\lambda(>0)$ for varied Da^{-1} when $\phi = 0.01$ and $\varepsilon = 1$ are shown in Figures 8-10. The increment of inverse Darcy number is contemplated to reduce these distributions which also implies the reduction in $\mathrm{Re}_L^{1/2} C_{fx}$, $2^{-1}\mathrm{Re}_L^{1/2} C_{fy}$ and $\mathrm{Re}_L^{-1/2} Nu_x$ when the flow is assisted through the mixed convection. Enlarging Da^{-1} would depreciate the permeability of the medium which becomes the reason towards such pattern of distribution.

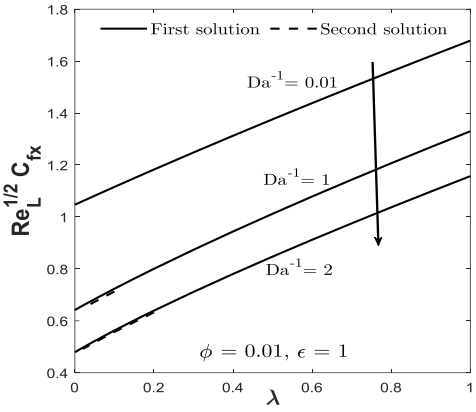

Fig. 8. Distribution of $\mathrm{Re}_L^{1/2} C_{fx}$ for different Da^{-1}.

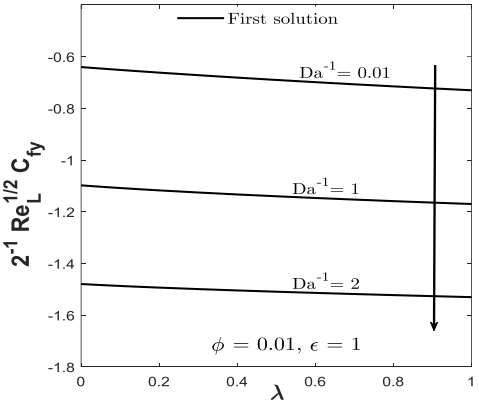

Fig. 9. Distribution of $2^{-1}\mathrm{Re}_L^{1/2} C_{fy}$ for different Da^{-1}.

In Figs. 11-18, we illustrate the impacts of volume fraction of $CoFe_2O_4$ and porosity parameter towards the three different velocity profiles which are the normal $h(\eta)$, tangential $h'(\eta)$ and circumferential (azimuthal) $g(\eta)$ velocities due to the cone geometry, and also the temperature profile $\theta(\eta)$.

The solutions in these figures suffice the boundary conditions which validate the precision of the

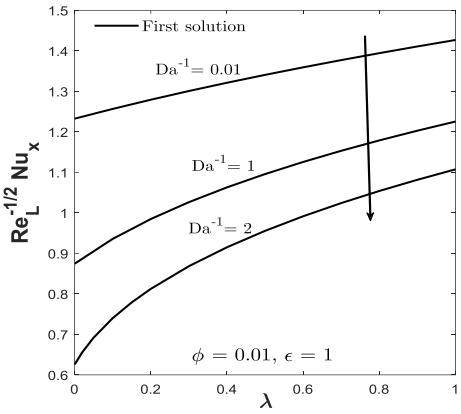

Fig. 10. Distribution of $\mathrm{Re}_L^{-1/2} Nu_x$ for different Da^{-1}.

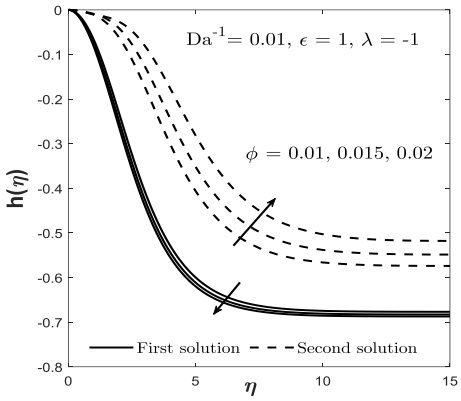

Fig. 11. Distribution of $h(\eta)$ for different ϕ.

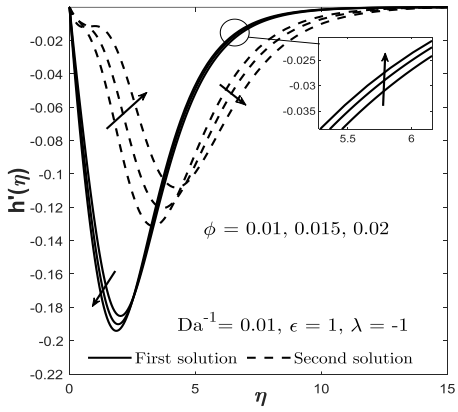

Fig. 12. Distribution of $h'(\eta)$ for different ϕ.

numerical solutions. In the context of the first solution, a more concentrated $CoFe_2O_4$ is depicted to decelerate all of the distributions but oppositely at a certain range of η for $h'(\eta)$ which is after the conflicting point, $\eta \approx 2.58$. The inclusion of $CoFe_2O_4$ increases the fluid thermal conductivity; hence this causes the heat transfer to occur more efficiently and reduces the temperature profile. The normal and circumferential velocities also decelerate due to the concentrated amount of $CoFe_2O_4$ that resists the flow movements.

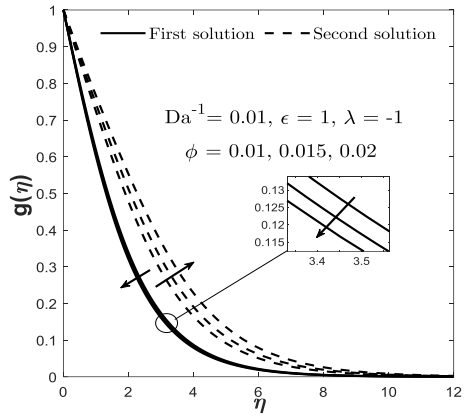

Fig. 13. Distribution of $g(\eta)$ for different ϕ.

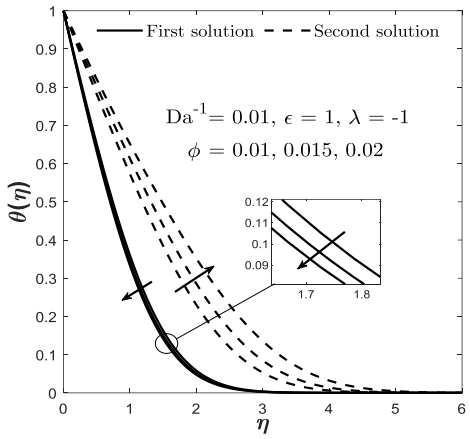

Fig. 14. Distribution of $\theta(\eta)$ for different ϕ.

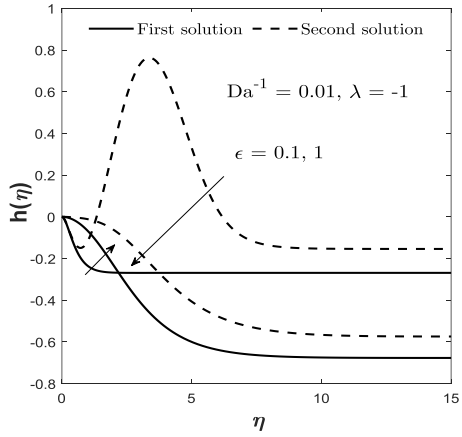

Fig. 15. Distribution of $h(\eta)$ for different ε.

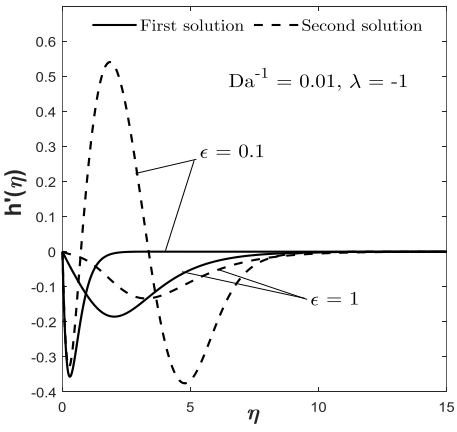

Fig. 16. Distribution of $h'(\eta)$ for different ε.

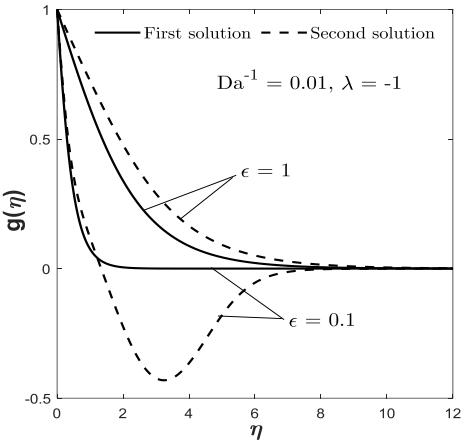

Fig. 17. Distribution of $g(\eta)$ for different ε.

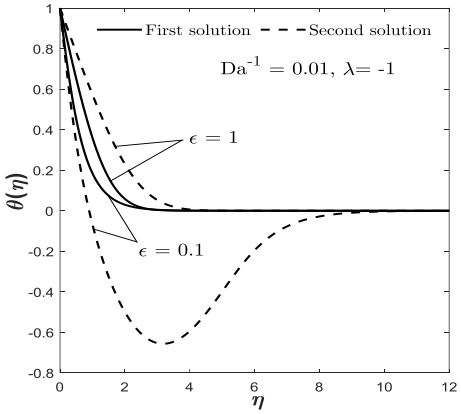

Fig. 18. Distribution of $\theta(\eta)$ for different ε.

Since we managed to generate dual solutions, especially for the opposing flow of mixed convection, it is necessary for us to conduct the stability analysis. The findings on the stability analysis is provided in Fig. 19 through the graphical illustration of the smallest eigenvalue γ_1 distribution against λ when $\phi = Da^{-1} = 0.01$, Pr = 6.96 and $\varepsilon = 1$. Initially, we already perceived the first solution to be stable as it is appeared to be the closest solution towards the boundary than the second solution when we look at the graph of the profiles in Figs. 11-18. However, this contemplation needs to be validated sophistically by generating the possible eigenvalues through a stability analysis. In Fig. 19, clearly, the first solution is stable as the generated smallest eigenvalue is positive due to the deterioration of perturbation. This analysis is also valid because as $\lambda \to \lambda_c$, $\gamma_1 \to 0$, meaning that, the perturbation is

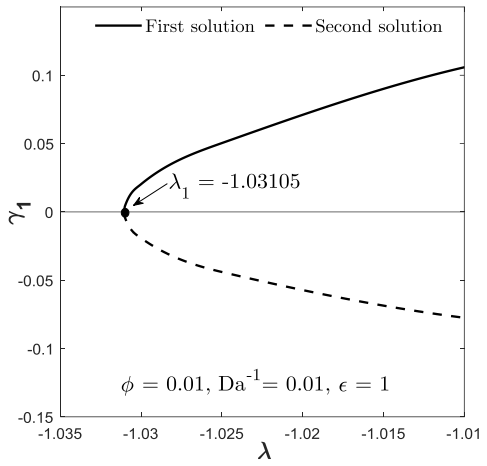

Fig. 19. Distribution of γ_1 against λ.

eventually decayed as time evolves for the stable solution.

Finally, although the incrementation of $CoFe_2O_4$ volume fraction up to 2% is estimated to augment the heat transfer rate as stated previously, the required work for the rotating cone is also increased due to the incrementation of the skin frictions which would result in a higher cost. Therefore, to achieve the optimum heat transfer performance, a ratio of change in the heat transfer rate to change in friction factor or also known as Thermal Performance Factor (TPF) is calculated to approximate the optimum required value for the $CoFe_2O_4$ volume fraction. The mathematical relation of TPF is expressed as follows (Kumar *et al*., 2016; Maradiya *et al*., 2018):

$$TPF = \frac{\left(Nu_x \,/\, Nu_{x0}\right)}{\left(f_c \,/\, f_{c0}\right)^{1/3}} \tag{29}$$

where the terms with subscript 0 denotes the respective initial value for the Nusselt number and friction factor. As we observed on our findings (refer Table 5), the TPF value is slightly higher when 1.5% volume fraction of $CoFe_2O_4$ is used compared to 2%. Hence, to have a lesser penalty of the required rotating work when increasing the volume fraction of $CoFe_2O_4$ in regard to augmenting the heat transfer, 1.5% volume fraction is preferable.

Table 5 TPF value due to the increment of ϕ when $\lambda = -1$, $\varepsilon = 1$ and $Da^{-1} = 0.01$

ϕ	1% to 1.5%	1% to 2%
TPF	0.984	0.972

6. CONCLUSION

The boundary layer flow and heat transfer of mixed convection MNF past a rotating vertical cone in a variable porosity regime have been scrutinized numerically. Stability analysis is also reported to complete the investigation. Based on the discussed findings, focusing on the opposing flow, we may conclude that:

- The heat transfer efficiency of the MNF can be magnified by controlling the volume fraction of MNP, mixed convection parameter, and porosity parameter.
- The ability of cobalt ferrite MNP in enhancing the heat transfer efficiency of MNF is proven in this study.
- The presence of a porosity regime increases the temperature of the MNF in the rotating cone and thickens the boundary layer thickness which causes the heat transfer rate to decrease.
- The transition of the boundary layer can be hindered by magnifying the volume fraction of MNP.
- Higher mixed convection magnifies the heat transfer, and the skin friction rates.
- The opposing flow of the mixed convection made the separation point of the boundary layer discoverable, and the existence of an alternative solution can be revealed.
- The alternative (second) solution is non-stable; hence the findings from this solution are not being recommended.

It should be noted that these present findings are only based on the respective MNF. For further investigation, other types of MNP such as magnetite and manganese-zinc ferrite can also be considered in the water/ethylene/methanol-based to analyze their flow and heat transfer behavior within the same geometry.

ACKNOWLEDGEMENT

The authors genuinely acknowledge Universiti Putra Malaysia, Universiti Teknikal Malaysia Melaka, and Ministry of Higher Education Malaysia (MOHE) for the Fundamental Research Grant Scheme (KPTFRGS/1/2019/STG06/IPM/02/3, Vot 5540309.

REFERENCES

Ahmadi, M. H., A. Mirlohi, M. Alhuyi Nazari and R. Ghasempour (2018). A review of thermal conductivity of various nanofluids. *Journal of Molecular Liquids* 265, 181–188.

Ahmed, N., A. Tassaddiq, R. Alabdan, U. Adnan, Khan, S. Noor, S. T. Mohyud-Din and I. Khan (2019). Applications of Nanofluids for the Thermal Enhancement in Radiative and Dissipative Flow over a Wedge. *Applied Sciences* 9(10), 1976.

Akilu, S., K. V. Sharma, A. T. Baheta and R. Mamat (2016). A review of thermophysical properties of water based composite nanofluids. *Renewable and Sustainable Energy Reviews* 66, 654–678.

Aladdin, N. A. L. and N. Bachok (2021). Duality Solutions in Hydromagnetic Flow of SWCNT-MWCNT/Water Hybrid Nanofluid over

Vertical Moving Slender Needle. *Mathematics* 9(22), 2927.

Ali, N., J. A. Teixeira and A. Addali (2018). A Review on Nanofluids: Fabrication, Stability, and Thermophysical Properties. *Journal of Nanomaterials* 2018, 1–33.

Anuar, N. S., N. Bachok and I. Pop (2021). Influence of MHD Hybrid Ferrofluid Flow on Exponentially Stretching/Shrinking Surface with Heat Source/Sink under Stagnation Point Region. *Mathematics* 9(22), 2932.

Bhandari, A. (2021). Unsteady flow and heat transfer of the ferrofluid between two shrinking disks under the influence of magnetic field. *Pramana* 95(2), 89.

Bognár, G. and K. Hriczó (2020). Numerical Simulation of Water Based Ferrofluid Flows along Moving Surfaces. *Processes* 8(7), 830.

Choi, S. U. S. and J. A. Eastman (1995). Enhancing thermal conductivity of fluids with nanoparticles. *ASME Fluids Engineering Division* 231, 99–106.

Colla, L., L. Fedele, M. Scattolini and S. Bobbo (2012). Water-Based Fe_2O_3 Nanofluid Characterization: Thermal Conductivity and Viscosity Measurements and Correlation. *Advances in Mechanical Engineering* 4, 674947.

Devendiran, D. K. and V. A. Amirtham (2016). A review on preparation, characterization, properties and applications of nanofluids. *Renewable and Sustainable Energy Reviews* 60, 21–40.

Gaviln, C. (2010). Turbulence, Vibrations, Noise and Fluid Instabilities. Practical Approach. In H. Woo (Ed.), *Computational Fluid Dynamics*. InTech.

Genc, S. and B. Derin (2014). Synthesis and rheology of ferrofluids: A review. *Current Opinion in Chemical Engineering* 3, 118–124.

Gul, A., I. Khan, S. Shafie, A. Khalid and A. Khan (2015). Heat Transfer in MHD Mixed Convection Flow of a Ferrofluid along a Vertical Channel. *PLOS ONE* 10(11), e0141213.

Guoxin, H., G. Xiwu, H. Hao, F. Haojie and W. Zheng (2008). Experimental studies on flow and pyrolysis of coal with solid heat carrier in a modified rotating cone reactor. *Chemical Engineering and Processing: Process Intensification* 47(9–10), 1777–1785.

Hamid, R. A., R. Nazar, K. Naganthran and I. Pop (2022). Dusty ferrofluid transport phenomena towards a non-isothermal moving surface with viscous dissipation. *Chinese Journal of Physics* 75, 139–151.

Harris, S. D., D. B. Ingham and I. Pop (2009). Mixed Convection Boundary-Layer Flow Near the Stagnation Point on a Vertical Surface in a Porous Medium: Brinkman Model with Slip. *Transport in Porous Media* 77(2), 267–285.

Hemmat Esfe, M., E. Hosseinizadeh and M. Mosaferi (2020). Investigation on nanofluid flooding effect on enhancement oil recovery process in a random pore distribution incomplete cone. *International Communications in Heat and Mass Transfer* 117, 104629.

Hering, R. G. and R. J. Grosh (1963). Laminar Combined Convection From a Rotating Cone. *Journal of Heat Transfer* 85(1), 29–34.

Jalili, B., P. Jalili, S. Sadighi and D. D. Ganji (2021). Effect of magnetic and boundary parameters on flow characteristics analysis of micropolar ferrofluid through the shrinking sheet with effective thermal conductivity. *Chinese Journal of Physics* 71, 136–150.

Jusoh, R., R. Nazar and I. Pop (2018). Magnetohydrodynamic rotating flow and heat transfer of ferrofluid due to an exponentially permeable stretching/shrinking sheet. *Journal of Magnetism and Magnetic Materials* 465, 365–374.

Karuppasamy, M., R. Saravanan, M. Chandrasekaran and V. Muthuraman (2020). Numerical exploration of heat transfer in a heat exchanger tube with cone shape inserts and Al2O3 and CuO nanofluids. *Materials Today: Proceedings* 21, 940–947.

Khairul, M. A., E. Doroodchi, R. Azizian and B. Moghtaderi (2017). Advanced applications of tunable ferrofluids in energy systems and energy harvesters: A critical review. *Energy Conversion and Management* 149, 660–674.

Khan, M. I., F. Alzahrani and A. Hobiny (2020). Simulation and modeling of second order velocity slip flow of micropolar ferrofluid with Darcy–Forchheimer porous medium. *Journal of Materials Research and Technology* 9(4), 7335–7340.

Khashi'ie, N. S., I. Waini, N. M. Ari and I. Pop (2021). *Unsteady squeezing flow of Cu-Al_2O_3/water hybrid nanofluid in a horizontal channel with magnetic field*. *Scientific Reports* 11(1), 14128.

Kierzenka, J. and L. F. Shampine (2001). A BVP solver based on residual control and the Maltab PSE. *ACM Transactions on Mathematical Software* 27(3), 299–316.

Kole, M. and S. Khandekar (2021). Engineering applications of ferrofluids: A review. *Journal of Magnetism and Magnetic Materials* 537, 168222.

Kolsi, L., S. Dero, L. A. Lund, U. F. Alqsair, M. Omri and S. U. Khan (2021). Thermal stability and performances of hybrid nanoparticles for convective heat transfer phenomenon with multiple solutions. *Case Studies in Thermal Engineering* 28, 101684.

Kumar, A., M. Kumar and S. Chamoli (2016). Comparative study for thermal-hydraulic performance of circular tube with inserts. *Alexandria Engineering Journal* 55(1), 343–349.

Kumar, A. and S. Subudhi (2018). Preparation, characteristics, convection and applications of magnetic nanofluids: A review. *Heat and Mass Transfer* 54(2), 241–265.

Kumari, M., I. Pop and G. Nath (1989). Mixed convection along a vertical cone. *International Communications in Heat and Mass Transfer* 16(2), 247–255.

Mabood, F. and A. T. Akinshilo (2021). Stability analysis and heat transfer of hybrid Cu-Al2O3/H2O nanofluids transport over a stretching surface. *International Communications in Heat and Mass Transfer* 123, 105215.

Mallikarjuna, B., A. M. Rashad, A. J. Chamkha and S. H. Raju (2016). Chemical reaction effects on MHD convective heat and mass transfer flow past a rotating vertical cone embedded in a variable porosity regime. *Afrika Matematika* 27(3–4), 645–665.

Maradiya, C., J. Vadher and R. Agarwal (2018). The heat transfer enhancement techniques and their Thermal Performance Factor. *Beni-Suef University Journal of Basic and Applied Sciences* 7(1), 1–21.

Marszałł, M. P. (2011). Application of Magnetic Nanoparticles in Pharmaceutical Sciences. *Pharmaceutical Research* 28(3), 480–483.

Maxwell, J. C. (1873). *A Treatise on Electricity and Magnetism.* Clarendon Press.

Merkin, J. H. (1986). On dual solutions occurring in mixed convection in a porous medium. *Journal of Engineering Mathematics* 20(2), 171–179.

Mohamed, M. K. A., N. A. Ismail, N. Hashim, N. M. Shah and M. Z. Salleh (2019). MHD Slip Flow and Heat Transfer on Stagnation Point of a Magnetite (Fe3O4) Ferrofluid towards a Stretching Sheet with Newtonian Heating. *CFD Letters* 11(1), 17–27.

Mohamed, M. K. A., S. H. M. Yasin and M. Z. Salleh (2021). Slip Effects on MHD Boundary Layer Flow over a Flat Plate in Casson Ferrofluid. *Journal of Advanced Research in Fluid Mechanics and Thermal Sciences* 88(1), 49–57.

Nayak, M. K., A. Patra, S. Shaw and A. Misra (2021). Entropy optimized Darcy-Forchheimer slip flow of Fe3O4−CH2OH2 nanofluid past a stretching/shrinking rotating disk. *Heat Transfer* 50(3), 2454–2487.

Nkurikiyimfura, I., Y. Wang and Z. Pan (2013). Heat transfer enhancement by magnetic nanofluids—A review. *Renewable and Sustainable Energy Reviews* 21, 548–561.

Palanisamy, K. and P. C. Mukesh Kumar (2019). Experimental investigation on convective heat transfer and pressure drop of cone helically coiled tube heat exchanger using carbon nanotubes/water nanofluids. *Heliyon* 5(5), e01705.

Prasad, A. R., D. S. Singh and D. H. Nagar (2017). *A Review on Nanofluids: Properties and Applications* 3(3), 25.

Purandare, P. S., M. M. Lele and R. K. Gupta (2015). Investigation on thermal analysis of conical coil heat exchanger. *International Journal of Heat and Mass Transfer* 90, 1188–1196.

Qasim, M., Z. H. Khan, W. A. Khan and I. Ali Shah (2014). MHD Boundary Layer Slip Flow and Heat Transfer of Ferrofluid along a Stretching Cylinder with Prescribed Heat Flux. *PLoS ONE* 9(1), e83930.

Raju, C. S. K., M. M Hoque, N. N. Anika, S. U. Mamatha and P. Sharma (2017). Natural convective heat transfer analysis of MHD unsteady Carreau nanofluid over a cone packed with alloy nanoparticles. *Powder Technology*, 317 408–416.

Raju, C. S. K. and N. Sandeep (2017). Unsteady Casson nanofluid flow over a rotating cone in a rotating frame filled with ferrous nanoparticles: A numerical study. *Journal of Magnetism and Magnetic Materials* 421, 216–224.

Rashad, A. M., B. Mallikarjuna, A. J. Chamkha and S. H. Raju (2016). Thermophoresis effect on heat and mass transfer from a rotating cone in a porous medium with thermal radiation. *Afrika Matematika*, *27*(7–8), 1409–1424.

Rasli, N. and N. Ramli (2021). Magnetohydrodynamic Flow and Heat Transfer Over an Exponentially Stretching/Shrinking Sheet in Ferrofluids. *Pertanika Journal of Science and Technology*, *29*(3).

Saidur, R., K. Y. Leong and H. A. Mohammed (2011). A review on applications and challenges of nanofluids. *Renewable and Sustainable Energy Reviews*, *15*(3), 1646–1668.

Saranya, S., Q. M. Al-Mdallal and S. Javed (2021). Shifted Legendre Collocation Method for the Solution of Unsteady Viscous-Ohmic Dissipative Hybrid Ferrofluid Flow over a Cylinder. *Nanomaterials* 11(6), 1512.

Shampine, L. F., I. Gladwell and S. Thompson (2003). *Solving ODEs with MATLAB* (1st ed.). Cambridge University Press.

Shampine, L. F., J. Kierzenka and M. W. Reichelt (2004). *Solving Boundary Value Problems for Ordinary Differential Equations in MATLAB with bvp4c. MATLAB File Exchange.*

Stephen, P. S. (1965). *Low viscosity magnetic fluid obtained by the colloidal suspension of magnetic particles* (Patent No. 3215572).

Sulochana, C., G. P. Ashwinkumar and N. Sandeep (2018). Boundary layer analysis of persistent moving horizontal needle in magnetohydrodynamic ferrofluid: A numerical study. *Alexandria Engineering Journal* 57(4), 2559–2566.

Takabi, B. and S. Salehi (2015). Augmentation of the Heat Transfer Performance of a Sinusoidal Corrugated Enclosure by Employing Hybrid Nanofluid. *Advances in Mechanical Engineering*, *6*, 147059.

Tshivhi, K. S. and O. D. Makinde (2021). Magneto-nanofluid coolants past heated shrinking/stretching surfaces: Dual solutions and stability analysis. *Results in Engineering* 10, 100229.

Uddin, Z., K. S. Vishwak and S. Harmand (2021). Numerical duality of MHD stagnation point flow and heat transfer of nanofluid past a shrinking/stretching sheet: Metaheuristic approach. *Chinese Journal of Physics* 73, 442–461.

Wahid, N. S., N. M. Arifin, N. S. Khashi'ie and I. Pop (2021). Mixed convection of a three-dimensional stagnation point flow on a vertical plate with surface slip in a hybrid nanofluid. *Chinese Journal of Physics* 74, 129–143.

Weidman, P. D., D. G. Kubitschek and A. M. J. Davis (2006). The effect of transpiration on self-similar boundary layer flow over moving surfaces. *International Journal of Engineering Science* 44(11–12), 730–737.

Yahaya, R. I., N. Md Arifin, S. S. P. Mohamed Isa and M. M. Rashidi (2021). Magnetohydrodynamics boundary layer flow of micropolar fluid over an exponentially shrinking sheet with thermal radiation: Triple solutions and stability analysis. *Mathematical Methods in the Applied Sciences* 44(13), 10578–10608.

Yu, W. and H. Xie (2012). A Review on Nanofluids: Preparation, Stability Mechanisms, and Applications. *Journal of Nanomaterials* 2012, 1–17.